Indian Journal of Pure & Applied Physics
Vol. 64, October 2026, pp. 1127-1136
DOI: 10.56042/ijpap.v64i10.31734

Innovative Design of a 5.3 GHz SAW Resonator for Next-Generation Electronic Systems

Baruna Kumar Turuk[a], Raushan Kumar[b], Radhanath Patra[c], Basudeba Behera[d] & Asisa Kumar Panigrahy[e*]

[a]Department Automation and Robotics Sandip Institute of Technology and Research Centre, Nashik 422 213, Maharashtra, India
[b]Department of Electronics and Communication Engineering, School of Engineering, SR University, Warangal 506 371, Telangana, India
[c]Department of Electronics and Communication Engineering, GIET University, Odisha 765 022, India
[d]Department of Electronics and Communication Engineering, National Institute of Technology Jamshedpur 831 014, India
[e]Department of Electronics and Communication Engineering, Faculty of Science and Technology, ICFAI Foundation for Higher Education Hyderabad, Hyderabad 501 203, India

Received: 19th May 2026; accepted: 29th July 2026

The swift expansion of fifth generation (5G) wireless technology demands high-performance radio frequency filters capable of operating at broader and higher frequency bands. 5G systems utilize frequencies from 3.0 to 6.0 GHz and millimetre waves. In this work, a multilayer single-port surface acoustic wave (SAW) device is presented based on a 128° YX-cut lithium niobate ($LiNbO_3$) piezoelectric material. The structure consists of a 500 nm-thick 128° YX-cut $LiNbO_3$ single-crystal substrate (500 nm $LiNbO_3$ film deposited on a 500 nm silicon layer and a 300 nm aluminium layer using spin coating). The proposed $LiNbO_3$/Al/Si multilayer SAW resonator operates at a resonance frequency of 5.3 GHz, achieving a quality factor of 250, a bandwidth of 20.8 MHz, and an electromechanical coupling coefficient of 3%. The device demonstrates an improved trade-off between bandwidth and resonator efficiency, making it a promising candidate for next-generation wireless communication systems. The results confirm that SAW devices using the 128° YX $LiNbO_3$/Al/Si multilayer structure offer excellent performance, making them suitable for 5G wireless communication systems.

Keywords: Surface acoustic wave (SAW), Finite element model (FEM), Microelectromechanical systems (MEMS), Fifth generation, Aluminum Nitride

1 Introduction

In recent years, mobile communication technology has advanced rapidly due to the introduction of 5G wireless systems[1]. To meet the rapidly growing demand for mobile data, it is necessary to have devices that can operate on a broader and higher range of communication frequencies. Acoustic wave devices play a vital role in mobile communication terminals, functioning as filters, duplexers, and sensors[2].

SAW devices have gathered significant interest due to their small dimensions, economical nature, consistent performance, and uncomplicated manufacturing methods[3]. Typically, SAW devices are manufactured on Substrate wafers made of $LiNbO_3$ or $LiTaO_3$. Nevertheless, the task of fabricating SAW devices with exceptional characteristics such as high frequency, wide bandwidth, and a high-quality factor on traditional bulk wafers is challenging[4]. Various design strategies have been explored to enhance the electromechanical coupling coefficient of wideband SAW filters, including material modification through ion implantation, structural refinement of inclined-angle film electrodes, and optimization of wafer orientation and cut angles. SAW devices utilising piezoelectric thin films that are securely mounted on a solid substrate have garnered significant interest due to their exceptional electromechanical coupling coefficient (k^2), adaptable frequency scalability, adjustable temperature coefficient of frequency (TCF), substantial power handling capacity, and straightforward manufacturing process suitable for large-scale production[5]. Due to its remarkably high k^2, lithium niobate ($LiNbO_3$) thin-film on the substrate is considered one of the most favourable materials for broadband applications, surpassing alternatives like aluminium nitride (AlN) and lithium tantalate ($LiTaO_3$)[6]. It is important to note that the properties of the acoustic mode in layered SAW devices, such as K^2, quality factor (Q), and phase velocity V_p are significantly influenced by both the substrate that is located underneath and the metallic electrode that is located above.

*Corresponding author: E-mail: asisa@ifheindia.org

To fully utilise the high k^2 property of $LiNbO_3$, it is necessary to create an Acoustic impedance contrast between the piezoelectric layer and substrate. This will improve the confinement of Elastic wave energy. Additionally, it is important to carefully specify the electrode material and thickness. The K^2 is the factor that determines the passband width of radio frequency (RF) filters that have a resonator structure[7]. The highest values of K^2 can be achieved by utilising certain rotated Y-cuts of $LiNbO_3$ with X-propagation as piezoelectric substrates. This study focuses on enhancing the K^2 by examining the lithium niobate at 128° YX cut orientation. A SAW resonator consists of several key elements: a substrate, a piezoelectric layer, interdigitated transducers (IDT), and a reflector or grating[8,9]. This study aims to design a multilayer SAW device to enhance bandwidth performance for 5G applications. The performance of a SAW resonator is strongly influenced by several key parameters, including the precise geometry of the IDTs, the separation between the reflectors and IDTs, the number of reflector elements, the spacing at the transducer ends, and the number of IDTs employed[10].

The finite element method (FEM) is utilized to analyze higher-order acoustic modes in slow-on-fast SAW devices built with $LiNbO_3$ films. Devices functioning within the 5 to 44 GHz range have been developed, exhibiting outstanding mass sensitivity and validating the platform's suitability for sensing at ultra-high frequencies[11-13]. The design of a multilayer one-port SAW resonator incorporates the following critical parameters.

The novelty of the proposed work lies in the development of a $LiNbO_3$/Al/Si multilayer SAW resonator operating at 5.3 GHz, which is specifically designed to achieve an improved balance between bandwidth, quality factor, and electromechanical coupling performance. Unlike conventional single-layer SAW resonators operating in the 5–6 GHz frequency range, the proposed multilayer structure utilizes optimized acoustic confinement and impedance matching through the incorporation of $LiNbO_3$, Al, and Si layers. This multilayer configuration enhances acoustic wave propagation characteristics and provides improved bandwidth performance while maintaining an acceptable quality factor.

Furthermore, the proposed design offers advantages in terms of frequency response optimization, resonator efficiency, and suitability for high-frequency wireless communication and 5G applications. To clearly demonstrate these improvements, a comparative analysis with previously reported 5–6 GHz SAW resonator designs has been added.

2 Related Work

Through the utilisation of SAW resonators with a variety of materials and cut orientations, several different strategies are being developed to improve the effectiveness of 5G communication. A large-coupling acoustic wave resonator was developed using a $LiNbO_3/SiO_2/Si$ functional substrate[12]. The designed model utilised a layered substrate consisting of a $LiNbO_3$ thin film deposited on an insulating layer. This design allowed for the creation and production of broadband RF and shear-horizontal SAW(SH-SAW) resonators. The main objective of this design was to achieve a significant effective k^2 of over 35 per cent near 1-GHz. An intermediate layer of silicon dioxide (SiO_2) was used to attach a thin film of single-crystalline LiNbO3 onto a silicon carrier wafer that was oriented in the (100) direction. This allowed for the construction of a hetero acoustic impedance waveguide that was both cost-effective and efficient. A SAW filter with a wide frequency range and low insertion loss characteristics was designed and implemented[14]. The filter was based on a 15° YX-$LiNbO_3/SiO_2/Si$ structure. The rapid advancement of RF technology has substantially increased data transmission in the 5G era, driving the need for SAW filters with enhanced bandwidth. This article introduces a multilayer structure consisting of a 15° YX-$LiNbO_3/SiO_2/Si$ configuration. The LN and SiO_2 films in this structure have consistent thickness and exhibit transparent interfaces. The undesired Rayleigh-mode–mediated resonance is mitigated by employing multi-level cascading system that regulates the thickness of the Cu electrode.

This study introduces a viable and efficient method for implementing Broadband, low-insertion-loss RF filters for 5G communication systems, which is suitable for widespread implementation and commercial use. High-frequency SAW devices were developed using a layered ZnO/SiC structure[15]. This device successfully produced ZnO piezoelectric films that were highly aligned on SiC substrates with a high sonic velocity. SAW devices based on a ZnO/SiC layered structure were successfully fabricated for the first time, achieving fundamental-mode operation up to 7 GHz. Experimental and theoretical analyses were performed to investigate the phase velocities (Vp), K^2,

and Q of one-port SAW resonators, under different ZnO normalised thicknesses (h/λ). A theoretical study presented the design of a layered SAW filter using a novel SiO_2/IDT/128°YX-$LiNbO_3$/diamond/silicon structure[16]. The study utilised the COMSOL Multiphysics software for modelling and simulation. The study employs a finite element analysis to examine the effects of $LiNbO_3$, an IDT, and SiO_2 thin films on the changes in phase velocity, (k^2), and temperature sensitivity of frequency. The fabricated longitudinal coupling resonator filter is analyzed transiently to determine its resonance properties and frequency response, revealing its SAW characteristics. A thorough examination of the simulation and measurement results of laterally induced shear bulk acoustic resonators (XBARs) in $LiNbO_3$ was conducted[17]. These resonators operated at a frequency of 5 GHz and exhibited high electromechanical coupling factors (kt^2) of up to 25 %. The resonators also had impedances close to 2 at resonance and anti-resonance, when loaded. Respective quality factors of 340 and 150 are achieved. This study presents the observed phenomena of major mode and spurious dispersion. Various geometric factors that impact the performance of resonators are examined to enhance the figure of merits (FoM) of the device for 5G filter applications. The majority of current methods for designing multilayer one-port SAW resonators involve utilising $LiNbO_3$ with varying cut orientations and spacing between the IDT and reflector. Therefore, the designed model will efficiently facilitate communication in the 5G network.

3 Proposed Methodology

SAW resonators are generally considered significant components for recent communication systems and their major function is that they either act as frequency synthesizers or filters. Working principle of the SAW resonator is the propagation of acoustic waves along the surface of the piezoelectric substrate. In a SAW resonator, acoustic waves are generated when electrical energy is injected through an IDT onto the piezoelectric material, where it is transformed into propagating mechanical waves, and the substrate, piezoelectric layer, IDT, and reflector or grating are included as the main components. The present work focuses on developing a multilayer one-port SAW resonator to improve bandwidth performance in 5G communication systems. Figure 1 presents the structural design of a one-port SAW resonator realized through the design procedure. In the initial step of the SAW resonator designing process, 500 nm thick lithium niobate piezoelectric film is deposited on 500 nm silicon and 300 nm aluminium using a spin coating process. Before that $LiNbO_3$ thin film is prepared using crystal growth technique. A thin film is obtained by melting pure lithium carbonate (Li_2CO_3) and niobium pentoxide (Nb_2O_5) powders in a platinum crucible. Following that 200 nm thick Molybdenum film is deposited over the piezoelectric substrate using the sputtering technique. This film forms the top and bottom electrode of IDT and the reflector. Further, the deposited Molybdenum film is patterned to achieve IDT fingers and reflector grating. The process of simulation and extraction of results for the proposed devices is reflected in the flowchart.

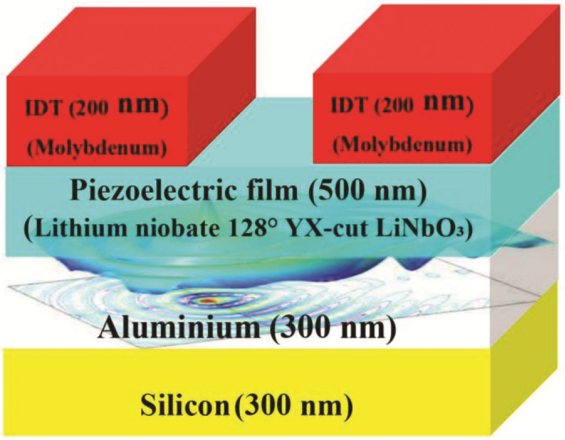


Fig. 1 — Structural Design of SAW Resonator

The parameters for one port SAW resonator are illustrated in Fig. 1 that consist of Distance between transducers and reflectors (LT) ranges from 0.5-1.5 nm, the Distance between the reflectors (LR) is 1.5 nm, the Width of aperture (W) is 5 nm, Number of IDT pairs (NT) is 60 pairs, Number of reflector pairs (NR) is 80 pairs. These are the parameters evaluated for designing a one-port SAW resonator. Figure 2 illustrates the complete COMSOL Multiphysics simulation workflow used for modeling and analyzing the proposed SAW resonator.

3.1 Mathematical Representation

SAW devices are subject to differential equations that require consideration of parameters such as device geometry, material properties, and boundary conditions to be solved. A numerical solution can be attained using the FEM, which is determined by the differential equations that correspond to the problem.

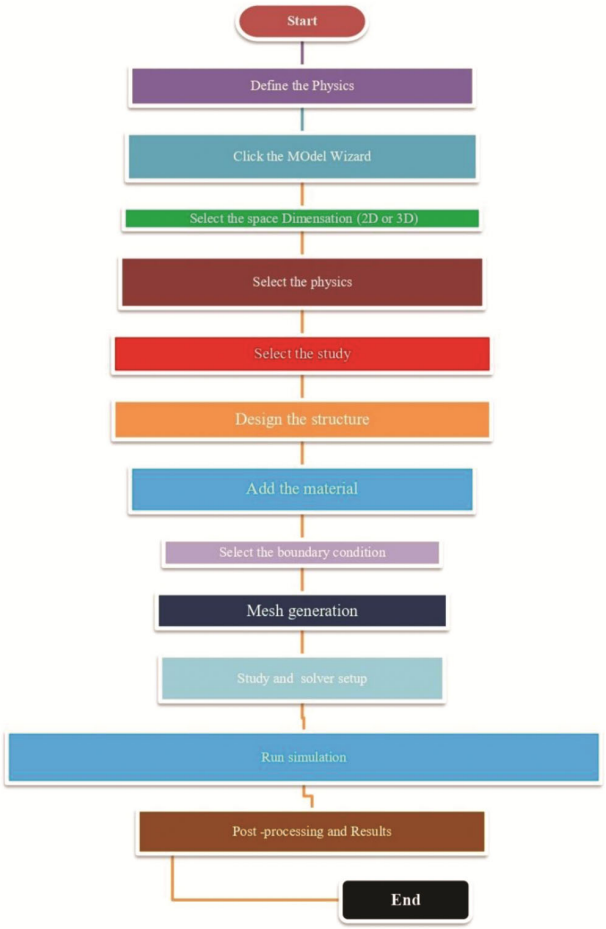


Fig. 2 — Flowchart illustrating the complete COMSOL Multiphysics simulation workflow for the proposed SAW resonator

In a piezoelectric crystal under stress, the interactions between mechanical stress, strain, electric field, and electric displacement are described by the following set of equations;

$$T_{ij} = C^{E}_{ijkl} S_{kl} - e_{ijk} E_k \quad \ldots (1)$$

$$D_i = e_{jkl} S_{kl} - \varepsilon^{S}_{ij} E_j \quad \ldots (2)$$

where T_{ij} is the stress vector, C_{ijkl} is the elasticity matrix (in units of N/m^2),e_{ijk} is the piezoelectric matrix (in units of C/m^2), ε_{ij} is the permittivity matrix (in units of F/m), E_k is the electric field vector (in units of V/m),S_{kl} is the strain vector, and D_i is the electrical displacement (in units of C/m^2).

The piezoelectric resonator can lose some of its energy while it is operating. Several different types of losses, including mechanical, dielectric, and piezoelectric, are experienced by the resonator. When dealing with an anisotropic material, it is necessary to consider a viscosity coefficient denoted as $\eta_c^{m,n}$ a dielectric loss factor denoted as $\eta_\varepsilon^{m,n}$ and a piezoelectric loss factor denoted as $\eta_e^{m,n}$ to account for the various losses that occur.

$$C_{ijkl}^{-m,n} = (1 + j\eta_c^{m,n}) C_{ijkl}^{m,n} \quad \ldots (3)$$

$$\varepsilon_{ij}^{-m,n} = (1 - j\eta_\varepsilon^{m,n}) \varepsilon_{ij}^{m,n} \quad \ldots (4)$$

$$e_{ij}^{-m,n} = (1 - j\eta_e^{m,n}) e_{ijk}^{m,n} \quad \ldots (5)$$

The components of each tensor are denoted by the parameters m and n.

Temperature fluctuations in a material give rise to two primary phenomena expansion or contraction of the material, and alterations in its physical properties. The coefficients for elasticityC_{ijkl}, piezoelectricity e_{kij}, permittivity ε_{kj}, and density (ρ) are adjusted based on temperature variations.

$$C_{ijkl}(T) = C_{ijkl}(T_0)[1 + \theta_1^C (T - T_0) + \theta_2^C (T - T_0)^2 + \cdots] \quad \ldots (6)$$

$$e_{kij}(T) = e_{kij}(T_0)[1 + \theta_1^e (T - T_0) + \theta_2^e (T - T_0)^2 + \cdots] \quad \ldots (7)$$

$$\varepsilon_{kj}(T) = \varepsilon_{kj}(T_0)[1 + \theta_1^\varepsilon (T - T_0) + \theta_2^\varepsilon (T - T_0)^2 + \cdots] \quad \ldots (8)$$

$$\rho(T) = \rho(T_0)[1 + \theta_1^\rho (T - T_0) + \theta_2^C (T - T_0)^2 + \cdots] \quad \ldots (9)$$

The thermal expansion coefficients (α_i) are highly responsive to changes in temperature. They characterise the increase in length dl/l in three spatial dimensions. The most common way to express changes in these parameters is through a Taylor series expansion.

$$\alpha_i(T) = \rho(T_0)[1 + \theta_1^{\alpha_i} (T - T_0) + \theta_2^{\alpha_i} (T - T_0)^2 + \cdots] \quad \ldots (10)$$

where, $\theta_1^C = \frac{1}{C_{ijkl}} \frac{dC_{ijkl}}{dT}$, $\theta_2^C = \frac{1}{2} \frac{1}{C_{ijkl}} \frac{d^2 C_{ijkl}}{dT^2}$, $\theta_1^e = \frac{1}{e_{kij}} \frac{de_{kij}}{dT}$, $\theta_2^e = \frac{1}{2} \frac{1}{e_{kij}} \frac{d^2 e_{kij}}{dT^2}$, $\theta_1^\varepsilon = \frac{1}{\varepsilon_{kj}} \frac{d\varepsilon_{kj}}{dT}$, $\theta_2^\varepsilon = \frac{1}{2} \frac{1}{\varepsilon_{kj}} \frac{d^2 \varepsilon_{kj}}{dT^2}$, $\theta_1^\rho = \frac{1}{\rho} \frac{d\rho}{dT}$, $\theta_2^\rho = \frac{1}{2} \frac{1}{\rho} \frac{d^2 \rho}{dT^2}$, $\theta_1^{\alpha_i} = \frac{1}{\alpha_i} \frac{d\alpha_i}{dT}$, $\theta_2^{\alpha_i} = \frac{1}{2} \frac{1}{\alpha_i} \frac{d^2 \alpha_i}{dT^2}$

The parameters (θ_1^c, θ_2^c), (θ_1^e, θ_2^e), (θ_1^ε, θ_2^ε), ($\theta_{1\rho}$, $\theta_{2\rho}$), and ($\theta_1^{\alpha_i}$, $\theta_2^{\alpha_i}$) correspond to the first- and second-order temperature-dependent coefficients for stiffness,

piezoelectric properties, permittivity, density, and thermal expansion, respectively. These coefficients must be obtained through experimental measurements, which can be both difficult and time intensive. In practical applications, it is often assumed that the dielectric and piezoelectric constants remain unaffected by temperature variations.

The resonance frequency of 5.3 GHz is maintained against variations caused by external factors such as temperature and mechanical stress through careful crystal orientation selection and multilayer structure optimization. The selection of the appropriate $LiNbO_3$ crystal orientation helps reduce the sensitivity of the acoustic wave velocity to temperature fluctuations, while the optimized multilayer structure improves mechanical stability and minimizes stress-induced frequency shifts. These design strategies contribute to enhanced frequency stability of the proposed SAW resonator. Furthermore, the quality factor (Q-factor) is an important parameter employed to evaluate the performance of the SAW resonator. A high Q-factor is desirable for high-performance SAW resonators and filters because it indicates lower energy loss within the device. Additionally, a high Q-factor produces a sharp resonance peak, enabling precise identification of the resonant frequency and improving the selectivity and overall performance of the device

4 Results and Discussion

The COMSOL Multiphysics software was used to simulate the proposed model for designing a multilayer one-port saw resonator using 128° YX cut-oriented $LiNbO_3$ for 5G communication. The purpose of the simulation was to validate the function and performance of the model. In the first step of the SAW resonator designing process, 500nm thick $LiNbO_3$ ate piezoelectric film is deposited on 300 nm aluminium and 500 nm silicon substrate. This multilayer saw resonator produces a high-performance filter for mobile communication. Before that $LiNbO_3$ thin film is prepared using crystal growth technique. Pure powders of Li_2CO_3 and Nb_2O_5 are melted in a platinum crucible to form $LiNbO_3$ thin film. Subsequently, a 200 nm thick layer of Molybdenum is applied onto the piezoelectric substrate using the sputtering technique. This film forms the top and bottom electrode of IDT and the reflector. Further, the deposited Molybdenum film is patterned to achieve IDT fingers and reflector grating[8]. The simulation software used for the analysis, namely COMSOL Multiphysics 5.4, along with the relevant physics interfaces employed for the SAW device modelling. The material properties of the constituent layers, including density, elastic constants, piezoelectric coefficients, and dielectric constants, which have been summarized in a dedicated Tables 1 and 2. The boundary conditions and meshing strategy adopted in the finite element simulations, including the treatment of the substrate, electrodes, and periodic boundary conditions. The equations used to calculate the quality factor (Q) and electromechanical coupling coefficient (k^2), along with appropriate references. The electromechanical coupling coefficient was calculated from the resonance and anti-resonance frequencies using the Eq. (12) in and

Table 1 − Properties of Anisotropic material lithium niobate at 128° YX cut orientation, Aluminium and Silicon

Property	128° YX-Lithium Niobate ($LiNbO_3$)	Aluminum (Al)	Silicon (Si)
Density, ρ (kg/m³)	4647	2700	2330
Relative Permittivity, $\varepsilon_{11}/\varepsilon_0$	85.2	1	11.7
Relative Permittivity, $\varepsilon_{33}/\varepsilon_0$	28.7	1	11.7
Young's Modulus, E (GPa)	203	70	169
Poisson's Ratio, ν	0.30	0.33	0.28
Elastic Constant C_{11} (GPa)	203	106	165.7
Elastic Constant C_{12} (GPa)	57.3	60	63.9
Elastic Constant C_{13} (GPa)	75.2	60	63.9
Elastic Constant C_{33} (GPa)	242.4	106	165.7
Elastic Constant C_{44} (GPa)	59.5	28.3	79.6
Piezoelectric Constant e_{15} (C/m²)	3.7	—	—
Piezoelectric Constant e_{22} (C/m²)	2.5	—	—
Piezoelectric Constant e_{31} (C/m²)	0.23	—	—
Piezoelectric Constant e_{33} (C/m²)	1.33	—	—
SAW Velocity (m/s)	≈3990	—	—

Table 2 — Boundary conditions and interface constraints employed in the finite element simulation of the proposed $LiNbO_3$/Al/Si one-port SAW resonator

Boundary/Region	Applied Boundary Condition	Purpose/Description
Bottom surface of Si substrate	Fixed Constraint (u = 0)	Simulates a semi-infinite substrate and suppresses rigid body motion
Top surface of IDT electrodes	Electrical Terminal (V = V_0)	Applies the input excitation voltage to the transmitting IDT
Ground electrode	Ground (V = 0)	Provides electrical reference potential
Free surfaces (non-electrode regions)	Free/Traction-Free Boundary	Allows natural propagation of surface acoustic waves
Lateral boundaries of the unit cell	Periodic Boundary Condition (Floquet Periodicity)	Models the periodic nature of the SAW resonator structure
Non-electrode surfaces	Electrical Insulation (n·D = 0)	Prevents charge leakage and enforces electrical isolation
Piezoelectric layer/electrode interfaces	Continuity Condition	Ensures continuity of displacement and electric potential
Substrate/piezoelectric interfaces	Continuity Condition	Maintains mechanical and electrical coupling between layers
Perfectly Matched Layer (PML)	Absorbing Boundary Condition	Minimizes artificial reflections from domain boundaries

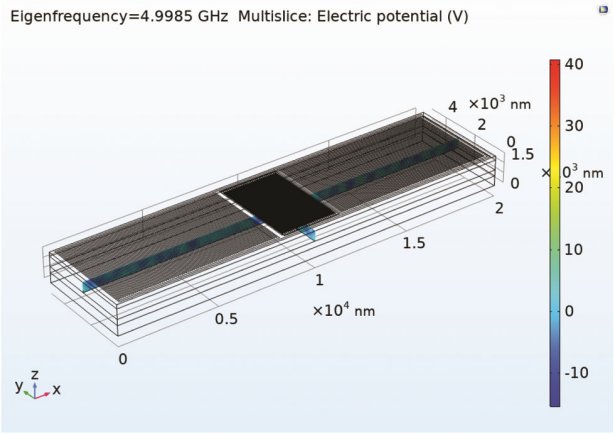


Fig. 3 − Three-dimensional view of the complete $LiNbO_3$-based resonator showing the electric potential distribution at the resonant Eigen frequency of 4.9985 GHz. The color scale represents the electric potential (V), illustrating the spatial distribution of the resonant mode across the device

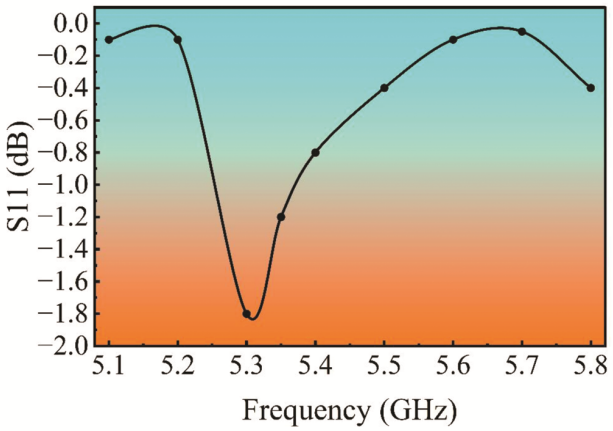


Fig. 4 − Simulated S_{11} parameter of the one-port SAW resonator as a function of frequency, showing a resonance at approximately 5.3 GHz with a minimum return loss of about −1.8 dB

quality factor is found using Eq. (14).

Figure 3 shows the $LiNbO_3$-filled resonator. The one-port SAW resonator's admittance, S_{11} parameters, coupling coefficient (k^2), quality factor, and phase velocity are calculated using this model. The simulated and measured S_{11} curves for the one-port resonator with λ of 0.6 nm are shown in Fig. 4 for frequencies from 5 GHz to 5.8 GHz. The frequency characteristics of one-port SAW resonators display a distinct resonance peak associated with the device. The electrical behavior of the SAW resonator is assessed using the impedance, Z. By analyzing how the impedance varies with frequency, both the resonance and anti-resonance frequencies can be identified. The relationship is expressed as $Z = V / (j\omega q)$, where V represents the electric potential, ω is the angular frequency, and q denotes the electric charge. In this case, the anti-resonance frequency (fa) is observed at 5.5 GHz, while the resonance frequency (fr) is at 5.3 GHz.

Figure 5 illustrates the admittance graph of the one-port SAW resonator. The admittance is used to measure the flow of current in the circuit and it is a reciprocal of the impedance. The unit of admittance is Siemens (S). Admittance is like impedance which consists of complex numbers such as real and imaginary parts. The real part denotes the conductance (G) and the imaginary part denotes the

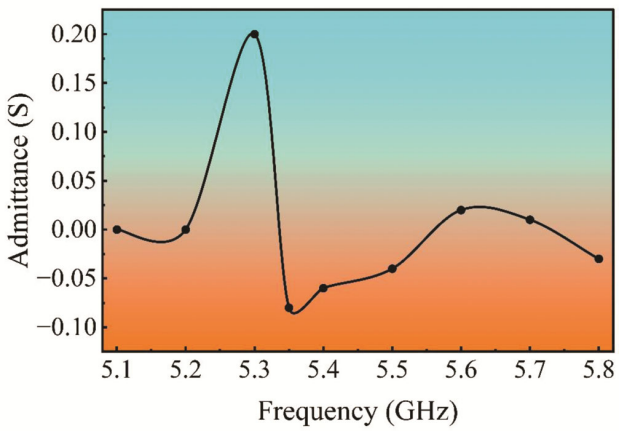


Fig. 5 — Admittance characteristics of one port SAW resonator

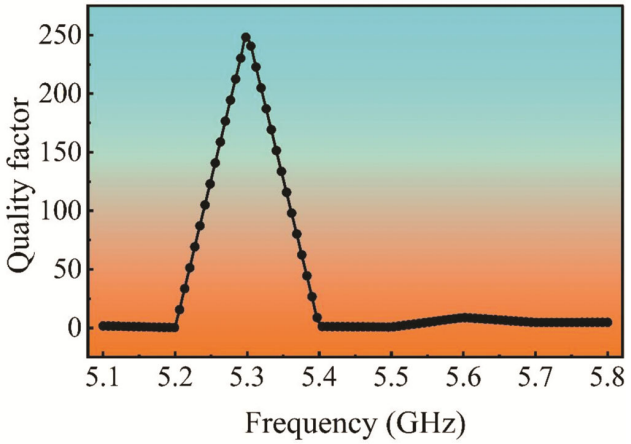


Fig. 6 — Quality factor vs frequency for one port SAW resonator

susceptance (B). The calculation of the admittance is derived by using, $Y=G+jB$. The conductance (G) of the one port SAW resonator is 0.21 S and the susceptance (B) of the SAW is -0.1S.

Figure 6 illustrates the graph of quality factor vs frequency for one port SAW resonator. In a SAW resonator, the Q factor is a dimensionless parameter that describes how underdamped the device is, defined as the ratio of the initial energy stored to the energy lost per radian of oscillation

$$Q = \left|\frac{Im(if)}{2Re(if)}\right| \quad \ldots (11)$$

For the proposed model, the quality factor measured at the resonance frequency of 5.3 GHz reaches a value of 250, representing the maximum point in the quality factor's frequency spectrum.

The relationships between the quality factor and the thickness of $LiNbO_3$ are depicted in Fig. 7. This section examines how the propagation velocity (v),

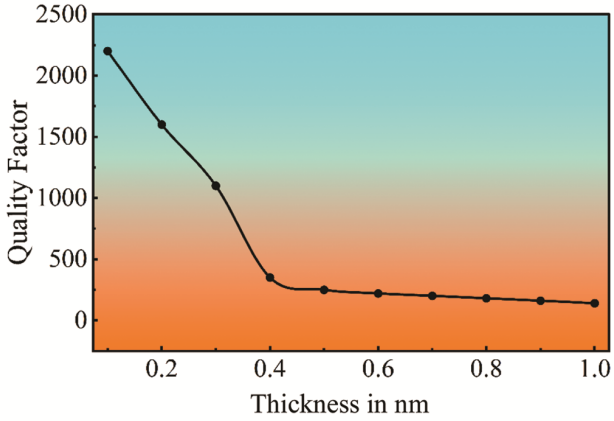


Fig. 7 — Quality factor vs thickness of $LiNbO_3$

the electromechanical coupling coefficient (k^2), and the quality factor (Q) change with respect to the normalized thickness, defined as $kh = 2\pi h/\lambda$, where h is the thickness of the $LiNbO_3$ layer and λ is the acoustic wavelength. The graph illustrates that as the thickness of the $LiNbO_3$ layer increases, the quality factor correspondingly decreases.

As shown in Fig. 6 and the comparative analysis presented in Table 3, the proposed $LiNbO_3$/Al/Si multilayer SAW resonator operates at a resonance frequency of 5.3 GHz with a quality factor of 250 and a bandwidth of 20.5 MHz. Compared with previously reported SAW resonators operating in the 5–6 GHz frequency range, the proposed device demonstrates a favourable balance between bandwidth and resonator efficiency. Conventional single-layer SAW resonators generally exhibit either a high Q-factor with a narrow bandwidth or a broader bandwidth accompanied by a reduction in the quality factor. In contrast, the proposed multilayer structure provides enhanced bandwidth while maintaining an acceptable Q-factor through improved acoustic confinement and optimized electromechanical coupling.

$$Q=\frac{f_c}{BW}$$

These characteristics indicate that the proposed multilayer SAW resonator achieves an effective trade-off between frequency response and resonator performance, making it a promising candidate for high-frequency wireless communication and 5G applications. The corresponding comparison and discussion have been incorporated into the revised manuscript and are presented in Fig. 6 and Table 3.

The quality factor for the thickness of 0.2 nm, 0.4 nm, 0.6 nm, 0.8μm and 1nm are 1500, 350, 200, 200

Table 3 — Performance comparison of the proposed $LiNbO_3$/Al/Si multilayer one-port SAW resonator with recent studies

References	Frequency (GHz)	Quality factor	Electro-Mechanical coupling coefficient (%)	Figure of Merit (FOM)	Bandwidth (MHz)
[18]	2	3300	6.5	215	.6
[15]	2	1000	10.5	105	2
[19]	2	2500	37.5	937.5	8.00×10^{-4}
[20]	1	3000	0.05	150	3.33×10^{-4}
[21]	2.43	130	0.2	26	1.8×10^{-2}
[22]	2	2500	7	175	8.00×10^{-4}
[23]	1	58	12	696	1.71×10^{-2}
[24]	2	230	7.07	1626.1	8.69×10^{-3}
Proposed Device	5.3	250	0.03	7.5	20.8

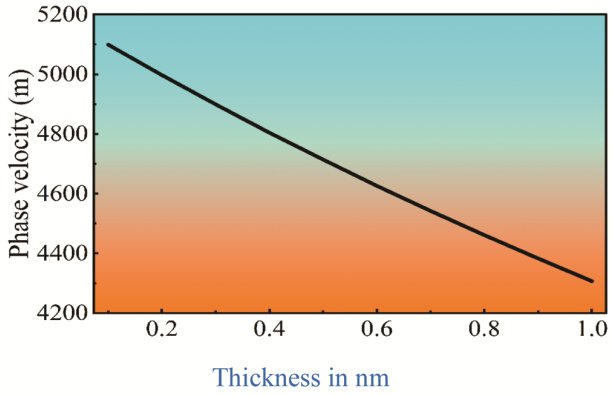


Fig. 8 — Phase velocity dispersion curve versus normalised $LiNbO_3$ thickness

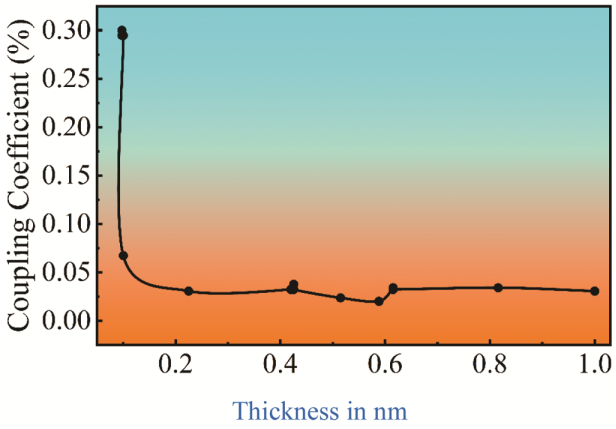


Fig. 9 — Variation of the electromechanical coupling coefficient with respect to the thickness of the $LiNbO_3$ layer is depicted through dispersion curves

and 150. Figure 8 illustrates the graph for phase velocity and $LiNbO_3$ thickness. The phase velocity of the one-port SAW resonator varies with the thickness of the lithium niobate. This graph is plotted Rayleigh using the wave phase velocity formula v = λ f where λ=0.6 nm and frequency is varied for each thickness of the lithium niobate. Phase velocity for the thickness of 0.2 nm, 0.4 nm, 0.6nm, 0.8 nm and 1nm are 5000 m/s, 4800 m/s, 4625 m/s, 4460 m/s and 4300 m/s respectively.

Figure 9 presents the dispersion curves showing how the electromechanical coupling coefficient varies with the thickness of the $LiNbO_3$ layer. For thickness values of 0.2 nm, 0.4 nm, 0.6 nm, 0.8nm, and 1nm, the coupling coefficient remains at 0.03. When the thickness ranges between 0.1 and 0.2, the coefficient decreases, after which it stabilizes and stays constant. The calculation of the electromechanical coupling coefficient is based on Eq. (12).

$$k^2 = \frac{\pi}{2}\left(\frac{fr}{fa}\right) tan\left[\frac{\pi}{2}\left(\frac{fa-fr}{fa}\right)\right] \quad \ldots (12)$$

The Figure of Merit (FOM) is calculated as the product of the electromechanical coupling coefficient and the quality factor, as expressed in Eq. (13).

$$\text{FoM} = \text{Quality factor} \times \text{coupling coefficient} \quad \ldots (13)$$

The bandwidth of the designed model is calculated using the given formula;

$$BW = fc/Q \quad \ldots (14)$$

where BW is the bandwidth, fc is the resonant frequency (Hz) and Q is the quality factor.

Table 3 illustrates the comparison of the proposed model and the existing resonators. The bandwidth of the designed model is determined by using the quality factor (Q) and the resonance frequency (fr). Thus, the bandwidth of the designed model is better compared to the existing techniques.

The comparison demonstrates that although several reported devices exhibit higher quality factors and electromechanical coupling coefficients, they primarily operate at relatively lower frequencies (1–2.43 GHz). In contrast, the proposed multilayer SAW resonator successfully operates at a higher frequency

of 5.3 GHz while maintaining acceptable performance metrics, making it suitable for emerging high-frequency wireless communication applications. The proposed design also offers the advantages of multilayer integration and compact device architecture.

The results indicate that while certain conventional piezoelectric substrates exhibit higher quality factors and electromechanical coupling coefficients, these devices generally operate at relatively lower frequencies. In contrast, the proposed $LiNbO_3$/Al/Si multilayer structure achieves operation at a higher resonance frequency of 5.3 GHz while maintaining acceptable values of Q and k^2, demonstrating its potential for high-frequency communication applications. The comparative analysis highlights the performance characteristics of the proposed structure relative to existing SAW resonator technologies and provides a clearer understanding of its advantages and limitations.

The thermal variation (temperature change) significantly affects the performance of a $LiNbO_3$/Al/Si multilayer SAW resonator.

i. Resonance Frequency (f_r): As temperature increases, the resonance frequency generally decreases due to thermal expansion and changes in the acoustic velocity of the materials. This effect is characterized by the Temperature Coefficient of Frequency (TCF).
ii. Electromechanical Coupling Coefficient (k^2): The electromechanical coupling coefficient experiences a slight reduction with increasing temperature because the piezoelectric properties of the $LiNbO_3$ layer change with temperature.

5 Conclusion

In this study, a multilayer one-port SAW resonator fabricated on 128° YX-cut $LiNbO_3$ is introduced to significantly improve the bandwidth of the designed model. The designed model consists of 500 nm thick $LiNbO_3$ piezoelectric film, which is deposited on the 500 nm silicon and 300 nm aluminium using a spin coating process for providing an enhanced electrical signal conversion from the input energy. Simulation of the designed model is operated on the wide frequency of 5-5.8 GHz, from that the resonance frequency of the designed model is 5.3 GHz. For the proposed model, the obtained quality factor and calculated electromechanical coupling coefficient (k^2) are 250 and 0.03, respectively. By employing a wide range of frequencies, the designed model achieves a bandwidth of 2.12×10^{-2}. This outcome demonstrates improved performance compared to existing models, which share a similar structure but differ in substrate materials and operating frequencies.

Although the proposed 5.3 GHz multilayer SAW resonator demonstrates improved performance in terms of bandwidth, quality factor, and electromechanical coupling, several research directions remain open for further investigation. Future work will focus on the experimental realization and validation of the proposed $LiNbO_3$/Al/Si multilayer SAW resonator through advanced microfabrication techniques and characterization methods. The influence of fabrication tolerances, residual stresses, and process-induced variations on the resonator performance will be systematically analyzed. Further studies will investigate the optimization of multilayer thicknesses, interdigital transducer (IDT) geometry, metallization ratio, and reflector configurations to achieve enhanced quality factor, reduced insertion loss, and improved frequency selectivity. The exploration of alternative piezoelectric and substrate materials, such as ScAlN, AlN, $LiTaO_3$, and SiC, will also be considered to improve electromechanical coupling and thermal stability at higher operating frequencies.

The primary challenges involve maintaining uniform film thickness, surface roughness, material composition, and interfacial adhesion across large substrates and multiple fabrication batches. Variations in spin speed, solution viscosity, solvent evaporation rate, ambient temperature, and humidity can result in non-uniform deposition of the piezoelectric and intermediate layers. Such non-uniformities may alter the acoustic wave propagation characteristics, leading to fluctuations in the resonance frequency and bandwidth.

Furthermore, thickness deviations in the multilayer structure can affect acoustic confinement and the electromechanical coupling coefficient, thereby influencing the quality factor (Q-factor) of the resonator. Surface defects, residual stresses, and interface imperfections introduced during large-scale fabrication may increase acoustic scattering and propagation losses, resulting in reduced resonator efficiency and degradation of the Q-factor. Additionally, batch-to-batch variations can affect the consistency of the bandwidth response, which is particularly important for communication and sensing applications.

Future work will focus on the experimental realization and validation of the proposed $LiNbO_3$/Al/Si multilayer SAW resonator using advanced

microfabrication and characterization techniques. The effects of fabrication tolerances, residual stresses, and process-induced variations on the resonator performance will be systematically investigated to evaluate device reliability and reproducibility

References

1 Kim J, Jang Y & Ahn D, *J Electr EngTechnol*, 20 (2025) 3517.
2 Takai T, Iwamoto H, Takamine Y, Fuyutsume T, Nakao T, Hiramoto M, *et al*., *IEEE Trans Ultrason Ferroelectr Freq Control*, 66 (5) (2019) 1006.
3 Turuk B K & Behera B, *Ferroelectr*, 583 (1) (2021) 33.
4 Yan Y, Huang K, Zhou H, Zhao X, Li W, Li Z, *et al*., *ACS Appl Electron Mater*, 1 (8) (2019) 1660.
5 Nagmani A K, Turuk B K & Behera B, *AIP Conf Proc*, 2341 (1) (2021) 020057.
6 Inoue S & Solal M, *IEEE Int Ultrason Symp*, Glasgow, UK, 2019, pp. 2079-2082, doi: 10.1109/ULTSYM. 2019.8925592.
7 Ke H, Shan Q, Qin P & Han T, *IEEE Int Ultrason Symp*, Glasgow, UK, 2019, pp. 2549-2552, doi: 10.1109/ULTSYM.2019.8925687.
8 Hashimoto K Y, *Surface Acoustic Wave Device Telecommun*, Springer-Verlag, Berlin Heidelberg, 116 (2000) 1.
9 Kadota M, Yunoki Y, Shimatsu T, Uomot M & Tanaka S, *IEEE Int Freq Control Symp*, Olympic Valley, CA, USA, 2018, pp. 1-4, doi: 10.1109/FCS.2018.8597496.
10 Turuk B K, Sahoo G, Nagmani A K & Behera B, *Natl Conf Electron Commun Comput*, (2020) 1.
11 Zhou J, Zhang D, Liu Y, Zhuo F, Qian L, Li H, Fu YQ & Duan H, *Engineering*, 20 (1) (2023) 112.
12 Hsu T-H, Tseng K-J & Li M-H, *IEEE Electr Device Lett*, 41 (12) (2020) 1825.
13 Grate J W, Martin S J & White R M, *Anal Chem*, 65 (1993) 940A.
14 Su R, Shen J, Lu Z, Xu H, Niu Q, Xu Z, Zeng F, *et al*., *IEEE Electr Device Lett*, 42 (3) (2021) 438.
15 Fu S, Wang W, Qian L, Li Q, Lu Z & Shen J, *IEEE Electr Device Lett*, 40 (1) (2018) 103.
16 Zhang H & Wang H, *Micromachine*, 12 (11) (2021) 1286.
17 Plessky V, Yandrapalli S, Turner P J, Villanueva L G, Koskela J & Hammond R B, *Electr Lett*, 55 (2) (2019) 98.
18 Behera B & Nemade H B, *Simulation*, 95 (2) (2019)117.
19 Sahoo G, Turuk B K & Behera B, *Trans Electr Electron Mater*, 24 (3) (2023) 242-249.
20 Sahoo G, Turuk B K, Behera B, *AIP Conf Proc*, 2341 (1) (2021) 020056.
21 Pijolat M, Loubriat S, Queste S, Mercier D, Reinhardt A, Defaÿ E, *et al.*, *Appl Phys Lett*, 95 (18) (2009) 182105.
22 Kimura T, Kadota M & Ida Y, *IEEE MTT-S Int Microw Symp*, Anaheim, CA, USA, 2010, pp. 1740-1743, doi: 10.1109/MWSYM.2010.5516895.
23 Rinaldi M, Zuniga C, Zuo C & Piazza G, *IEEE Trans Ultrason Ferroelectr Freq Control*, 57 (1) (2010) 38.
24 Zhu X, Phillips J D & Mortazawi A, *IEEE MTT-S Int Microw Symp* (2007) p. 671.